Automatic Force-Compliant Robotic Ultrasound Screening of Abdominal Aortic Aneurysms

Salvatore Virga*[1,2], Oliver Zettinig*[1], Marco Esposito[1], Karin Pfister[3], Benjamin Frisch[1], Thomas Neff[2], Nassir Navab[1,4] and Christoph Hennersperger[1]

***Abstract*— Ultrasound (US) imaging is commonly employed for the diagnosis and staging of abdominal aortic aneurysms (AAA), mainly due to its non-invasiveness and high availability. High inter-operator variability and a lack of repeatability of current US image acquisition impair the implementation of extensive screening programs for affected patient populations. However, this opens the way to a possible automation of the procedure, and recent works have exploited the use of robotic platforms for US applications, both in diagnostic and interventional scenarios. In this work, we propose a system for autonomous robotic US acquisitions aimed at the quantitative assessment of patients' vessel diameter for abdominal aortic aneurysm screening. Using a probabilistic measure of the US quality, we introduce an automatic estimation of the optimal pressure to be applied during the acquisition, and an online optimization of the out-of-plane rotation of the US probe to maximize the visibility of the aorta. We evaluate our method on healthy volunteers and compare the results to manual acquisitions performed by a clinical expert, demonstrating the feasibility of the presented system for AAA screening.**

I. INTRODUCTION

Ultrasound (US) imaging has become the first-line imaging modality for multiple medical indications, including the focused assessment with sonography for trauma (FAST) as a routine emergency workflow or general vascular conditions [1], [2]. Due to its non-invasiveness and swift imaging capabilities, ultrasound is well suited for screening applications. One target area with a high associated benefit from routine screening would be the abdominal aortic aneurysm (AAA), a dilation (ballooning) of one of the major vessels in the human body. The major risk of an AAA is the rupture of the aneurysm, which is associated with high mortality rates up to 50%. The probability for rupture depends on the size, shape and stress of the aneurysm, with a substantially increased risk for diameters above 6 cm [3]. Ultrasound is already employed as a standard diagnostic tool for the imaging of the aorta, and US-based staging is widely accepted in clinical practice [4]. However, challenges with respect to inter-operator variability and standardized measurement approaches still impair the implementation of national or international sonography-based screening programs [4], [5], [6]. In contrast to conventional clinical 2D ultrasound, 3D US showed an improved localization of aneurysm-shape and endoleak after Endovascular Aortic Repair (EVAR) compared to 2D US, using contrast-enhanced imaging [7]. Based on the extraction of quantitative values from these data, a 3D ultrasound scanning system with reproducible and constant acquisition quality could facilitate the establishment of screening frameworks. While the patient benefit from an early detection and regular check for aortic aneurysms is obvious in such a program, discussions about the overall cost-effectiveness of potential screening activities remain [8]. The full automation of the acquisition using robotic technology would reduce personnel costs a major factor for the data acquisition while achieving full comparability of acquired data. In addition, work-related musculoskeletal discomfort of US examiners could be reduced [9].

In the past decades, attempts for generating operator-independent 3D ultrasound data focused on motorized probes [10], freehand 3D approaches [11], partially also combined with ECG-gating [12] and more recently pulse-oximetry [13] to remove artifacts due to vessel pulsation. While today's methods achieve higher repeatability of the acquired data, they lack an automation of the acquisition itself. In view of servoing approaches, US probes are used and guided by robotic systems for needle placement [14], as well for showing a constant anatomical position by breathing compensation [15], an automatic optimization of the US probe direction for optimal acoustic coupling [16] and the automatic servoing based on live image registration [17]. Finally, first attempts for fully automated ultrasound acquisitions used RGB skin feature detection following a rigid acquisition protocol for liver ultrasound [18], and performed acquisitions based on previously planned trajectories on tomographic image data [19].

In this work, we present a fully autonomous framework to acquire abdominal 3D US images to facilitate AAA screening in clinical routine. Designed to cope with a high anatomical variety in the general population, our system aims to adapt the performed US trajectory to the individual patient. To this end, we elastically register the patient to a generic MRI-based atlas, and autonomously perform a force-optimized robotic US scan of the abdominal aortic region, allowing for manual diameter measurements. In particular, our contributions are as follows:

a) In contrast to [19], a deformable registration in combination with a generic patient atlas is employed to account for various body sizes and shapes. In this way, patients for whom no tomographic imaging data is available can

*These authors contributed equally to this work.

[1]Computer Aided Medical Procedurs, Technische Universität München, Munich, Germany. salvo.virga@tum.de

[2]KUKA Roboter GmbH, Augsburg, Germany

[3]Division of Vascular and Endovascular Surgery, University Medical Center Regensburg, Regensburg, Germany

[4] Computer Aided Medical Procedures, Johns Hopkins University, Baltimore, MD, USA

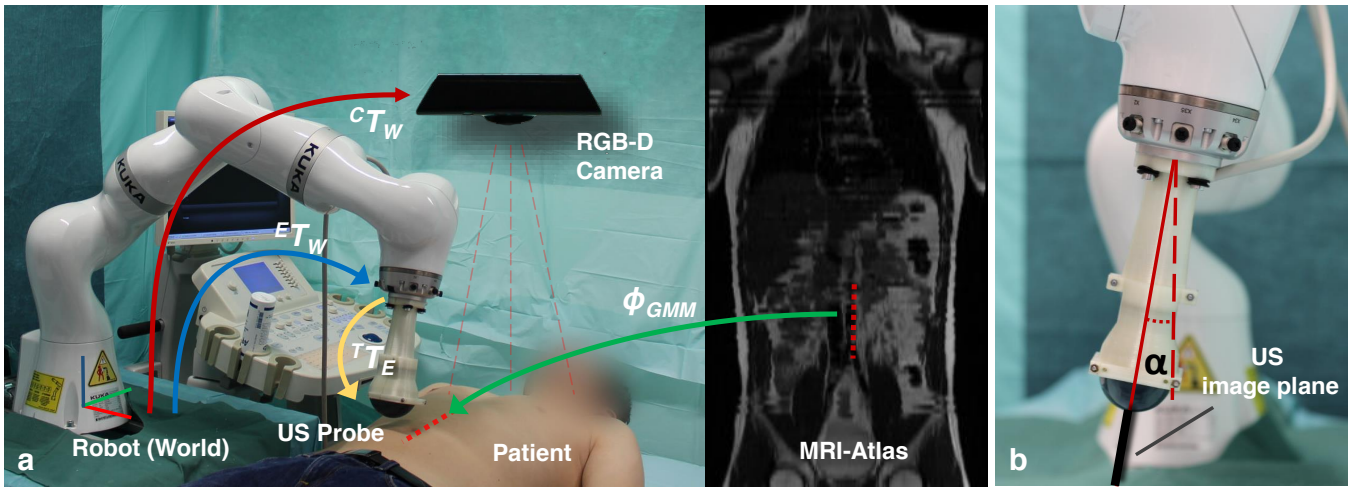

Fig. 1. **a)** System setup showing the robot, the US transducer mounted to its end-effector, the RGB-D camera on the ceiling, the patient, a coronal slice of the MRI atlas, and all required transformations, including the camera-to-robot (${}^{C}T_{W}$) and extrinsic US probe calibrations (${}^{T}T_{E}$). The red-dotted line indicates the scan trajectory. **b)** Close-up of the US transducer, showing the US imaging plane (*thick black line*) and the out-of-plane rotation angle α.

undergo the proposed screening protocol.

b) Similarly, due to the great variety of possible patient conditions, there is a need for an adaptive parametrization of the employed contact force of the US transducer onto the skin [4]. In this work, we propose to utilize confidence maps [20] to automatically determine the optimal force for the US scan.

c) Finally, we propose a control law based on confidence maps as an adapted version of [16] targeted at our application. In this regard, we initially estimate and continuously adjust the out-of-plane rotation of the US transducer during the acquisition. This enables the optimization of the image quality at specified penetration depths (e.g. aorta), compensating for shadowing artifacts due to the presence of bowel gas.

II. METHODS

The presented autonomous screening system consists of a robotic manipulator, allowing for force estimation at its end-effector by means of internal joint torque sensors, and a rigidly attached US transducer. In addition, a structured-light RGB-D camera is mounted at the ceiling of the examination room, as illustrated in Fig. 1a. In this section, we first describe the registration between the MR-atlas and the patient using RGB-D data in Sec. II-A. Then, we summarize in Sec. II-B how the signal loss in US images is estimated in the form of confidence maps. While in Sec. II-C, the overall robot control scheme is introduced, specific details concerning the force estimation and out-of-plane control are described in Sec. II-D and II-E, respectively.

A. Patient Registration and Trajectory Transfer

The aim of a global patient-to-world registration is to gather knowledge about the current patient position with respect to the system setup, so that accurate and safe motions of the robotic arm can be achieved. We exploit the sensing information of a RBG-D camera to transfer a generic trajectory aimed at the aorta of an atlas onto the current patient.

For camera-to-robot calibration, we employ a technique based on augmented reality markers similar to the approach in [19] to determine the transformation ${}^{C}T_{W}$ (cf. Fig. 1a). Note that the computer vision notation for transformations, i.e. 4×4 homogeneous matrices, are used in this work.

Given the wide target population of a screening program, it is not feasible to assume the availability of individual tomographic images for each patient. Hence, we propose to leverage a statistical MRI atlas based on physical and anatomical characteristics, such that the anatomy of each patient can be taken into account for the trajectory planning [21]. A surface point cloud P_{MRI} extracted from a selected MRI atlas image can be elastically registered to the live point cloud P_{RGBD} obtained from the RGB-D camera. We make use of an implementation of the Coherent Point Drift algorithm [22], a probabilistic non-rigid registration method that fits a Gaussian Mixture Model (GMM) to the moving point set. The GMM is initialized using the target points P_{RGBD} and a coherent velocity is enforced to its motion so that a smooth non-linear transformation $\Phi_{GMM} : \mathbb{R}^4 \rightarrow \mathbb{R}^4$ can be computed using spline interpolation. Both point sets are subsampled by a factor f_s for this process, allowing for an optimal trade-off between the fitting accuracy and the computational performance.

By a projection of the start- and endpoint ($\mathbf{p}_s$,$\mathbf{p}_e \in \mathbb{R}^4$) of the aortic region of interest from the atlas to its surface, the robotic trajectory on the patient surface ($\mathbf{p}'_s$,$\mathbf{p}'_e$) is obtained by transfering these points to the world coordinate system

$$\mathbf{p}'_s = {}^{C}T_{W} \cdot \Phi_{GMM}\left[f_{NN}(\mathbf{p}_s, \mathbf{e}_z)\right], \tag{1}$$

where $\mathbf{e}_z = (0, 0, 1, 0)$ is the vertical unit vector, and $f_{NN}(\mathbf{p}, \mathbf{n})$ computes the nearest element of the point cloud P_{MRI} to the ray $\mathbf{p} + \lambda\mathbf{n}, \lambda \in \mathbb{R}_0$ (analogous for $\mathbf{p}'_e$).

B. US Acquisition and Confidence Map Computation

In our framework, a series of 2D B-mode frames $I_i \in \mathbb{R}^2$ are acquired using a convex transducer suited for abdominal scans. For an estimation of the ultrasound quality, we employ confidence maps as introduced by [20]. In short, a graph is constructed between the pixels of the B-mode image, with source (1) and sink (0) nodes at the transducer elements and the bottom of the image, respectively, and edge weights based on the US intensities between pixels. The confidence map $C_i \in \mathbb{R}^2 \rightarrow [0,1]$ is then defined as the equilibrium diffusion solution, i.e. the probability of a random walk starting from a particular pixel to rather reach the transducer than the bottom (see Fig. 3a). We refer the reader to [23] for further details. For any given US frame, we denote with the feature

$$\zeta = \frac{1}{|R|} \sum_{(x,y)\in R} C(x,y), \tag{2}$$

the average confidence in the rectangular region R, centered around the estimated world-coordinate location of the aorta in the corresponding B-mode frame I. Since the spine and the aorta are almost incompressible, it can be estimated from the atlas as in Eq. 1 and considered constant regardless of the current force onto the patient. The averaging copes with the inherent level of noise in confidence maps [24].

C. Robot Control Scheme

The overall goal of the robot control scheme is threefold: First, the US sweep acquisition requires following a predefined trajectory on the patient. Second, the force exerted by the US transducer onto the tissue is intended to not only be sufficient but also optimal over time, achieving good acoustic coupling throughout the sweep. Third, the out-of-plane rotation needs to be adjusted on-line to maintain high image quality even in the presence of bowel gas, shadowing, and other artifacts. Considering the desired tool-tip pose

$$\mathrm{P}_d = \begin{bmatrix} \mathrm{R}(\alpha,\beta,\gamma) & \mathbf{t} \\ \mathbf{0} & 1 \end{bmatrix} \tag{3}$$

with translation $\mathbf{t} = (x,y,z)$ and rotation R using the Euler angles (α,β,γ), it is possible to decouple the three tasks. A standard position controller is used to command translations (x,y) in the horizontal plane, guided by the planned trajectory.

D. Adaptive Force Estimation

The downward translational component z is controlled by a force controller as already demonstrated in prior art [16], [17], [25]. Constant force control for manipulators with elastic joints is typically achieved by balancing external Cartesian forces $\mathbf{F_{ext}}$ acting on the end-effector with a desired force $\mathbf{F_d}$ so that $\mathbf{F_{ext}} - \mathbf{F_d} = 0$, as historically described in [26]. For real-time behavior, torque sensors in all robotic joints are utilized to compute the external forces using both the Jacobian and the known inverse dynamics system of the manipulator.

Although the area of general robotic force control has been extensively discussed throughout the last decades, the choice of an appropriate force $\mathbf{F_d}$ for a particular medical scenario depended on a manual parametrization up to now. While too little pressure will compromise good acoustic coupling and sufficient image quality during US acquisitions, excessive force might overly deform the anatomy or even harm the patient. In the view of a fully autonomous robotic system for US screening, an optimal force value cannot be known a priori but has to be estimated online to cope with a variety of patients constitution and tissue density. Therefore, we propose an online adaptive force estimation based on confidence values presented in II-B. During initialization, we vertically approach the start pose $\mathbf{p}'_s$ until skin contact ($\mathbf{F_{d}}_0 = 0$). Next, the desired force exerted onto the tissue is increased iteratively by $\mathbf{F}_{step}$ until a mean confidence threshold Θ is reached (H is the Heaviside step function):

$$\mathbf{F_{d}}_{i+1} = \mathbf{F_{d}}_i + \mathbf{F}_{step} \cdot H\left(\Theta - \zeta_i\right). \tag{4}$$

E. Optimization of Out-of-Plane Rotation

The Euler angles (α,β,γ) of the pose P_d can be interpreted as out-of-plane rotation, in-plane rotation, and rotation around the transducer axis, respectively. Contrary to the target anatomies investigated in [16], [17], axial aortic scans benefit only marginally from in-plane or transducer axis rotation: On the one hand, turning the US probe around its axis does not avoid acoustic obstacles between the transducer and the aorta. On the other hand, an in-plane rotation during axial scans constitutes lateral tilting, quickly translates the aorta away from the image center, and is not considered helpful in clinical routine [7]. Thus, we define $\beta = \gamma = 0$ for all experiments and concentrate on the more challenging out-of-plane rotation α for image quality optimization.

Initially, a sweep is acquired with angles between $[\alpha_{min}; \alpha_{max}]$, where the confidence feature ζ_α is recorded for each rotatory pose. The optimal out-of-plane rotation α_0 for the start point of the sweep is then defined as the angle that maximizes confidence at the aorta: $\alpha_0 = \arg\max_\alpha \zeta_\alpha$.

Throughout the acquisition, we aim to maintain an optimal echoing pose. As the direction to tilt the probe out of its plane cannot be directly inferred from 2D frames, we propose to compute the following parameters for each frame. First, the binary parameter κ indicates a drop in confidence below the average of the preceding M frames

$$\kappa = H\left(\zeta_i - \frac{1}{M} \sum_{j=i-M-1}^{i-1} \zeta_j\right). \tag{5}$$

It is used to determine whether the current probe orientation provides sufficient image quality. Second, the parameter $s \in \{-1,1\}$, $s_0 = 1$, states the direction the probe should tilt to:

$$s_i = \begin{cases} -s_{i-1} & \text{if } \zeta_i < \zeta_{i-M} \ \wedge \left| \sum_{j=i-M-1}^{i-1} s_j \right| = M \\ s_{i-1} & \text{else .} \end{cases} \tag{6}$$

As a result, s will change sign only if there has not been a change in the previous M iterations, and the current

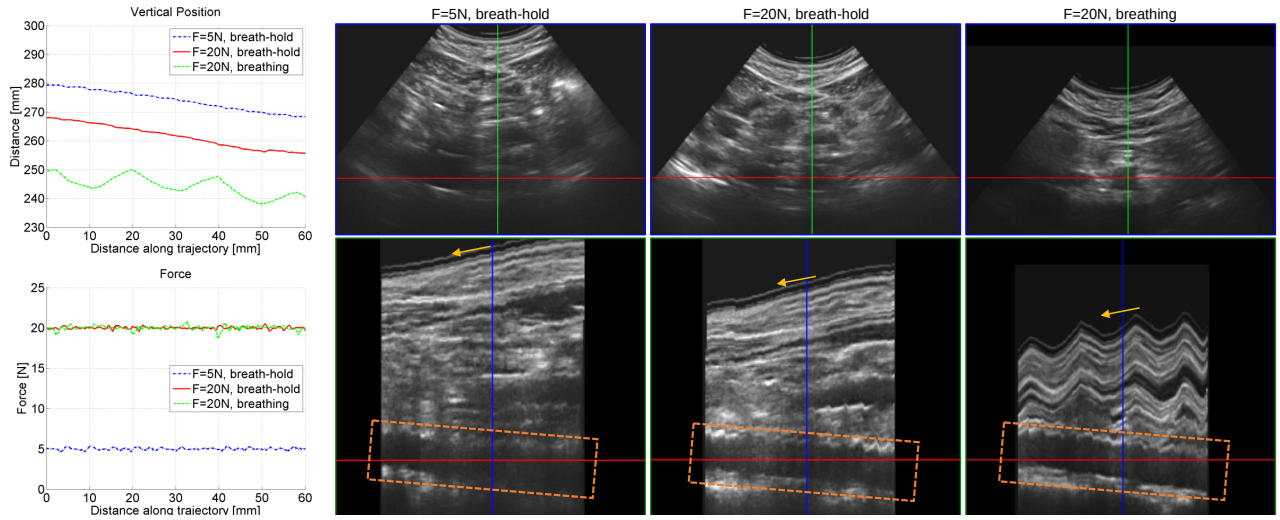

Fig. 2. Results of force adaptation experiments for one subject, including the measured vertical position of the transducer and the corresponding force (*figures on the left*), and axial (*top*) and sagittal (*bottom*) slices of the compounded US volumes. Without proper force onto the tissue (5 N experiment, *left image column*), the US quality at the aorta, in particular its posterior wall, is poor (*orange box*). Quality improves with the adaptive force estimation (20 N experiments, *center column*). Results also show that the force controller can successfully account for breathing motion and allows for steady aortic acquisitions, even if the US image of tissue directly underneath the skin becomes unusable (*right image column*). Yellow arrows indicate the scan direction.

confidence dropped below the one M iterations ago. Altogether, the desired out-of-plane rotation can be computed by combining these factors $\alpha_i = \alpha_{i-1} + \kappa \cdot s \cdot \alpha_{step}$. Updates of α as thus not continuous but are handled by the position controller in a smooth fashion as in [19].

III. EXPERIMENTS AND RESULTS

A. Material and Experimental Setup

The robotic manipulator used in this work is a KUKA LWR iiwa R800 (KUKA Roboter GmbH, Augsburg, Germany) with the KUKA Sunrise.Connectivity software package. A software module[1] developed by the authors allows a direct control of the robot functionalities via the Robot Operating System[2] (ROS) framework. The methods presented in Sec.II are implemented in custom ROS modules, which forward their control output to the KUKA robot controller. For US acquisition, an Ultrasonix® Sonix RP US system equipped with a 4DC7-3/40 curvilinear transducer (Analogic Corporation, Peabody, MA, USA) is used (frequency: 3.3 MHz, depth: 140 mm, gain: 50%). The US probe is attached to the robot flange using a custom designed holder (cf. Fig. 1b). Spatial and depth information are acquired using a Kinect camera (Microsoft Corporation, Redmond, WA, USA) placed above the patient. Experiments ran on a workstation (Intel Core i5, NVIDIA GTX 970) connected to the aforementioned systems. Medical image processing is performed within the ImFusion Suite 1.2.16 (ImFusion GmbH, Munich, Germany). The performed camera-to-robot calibration led to an average error of 2.46 ± 0.96 mm on the x-y plane and 6.42 ± 3.67 mm along the camera's depth axis.

We evaluated our method on five different healthy volunteers (age 24-27, 2 female, 3 male), scanning the aorta from slightly inferior of the rib cage in downward direction roughly until the navel (scanning time approx. 2 minutes per patient). The atlas consisted of a T2-weighted MR image (resolution $1.2 \times 1.2 \times 6$ mm) of one healthy individual (age 26, male), which was deemed sufficient for this volunteer study due to the similar anatomical condition. Similar to [19], the Hausdorff distance between P_{RGBD} and the warped atlas surface mesh was on average 3.7 mm (maximum 9.8 mm), robustly allowing the visualization of the aorta in the US frame without further compensation. For all experiments, the following set of parameters was used: $f_s = 0.01$, $\mathbf{F}_{step} = 2$ N, $\mathbf{F}_{max} = 25$ N, $\alpha_{step} = 2°$, $M = 4$ and the region R comprised an area of 10×10 px. The robot moved with $v = 5$ mm/$_s$ during sweeps, and Θ was empirically set to 0.2.

B. Validation of Force Estimation

For all subjects, patient registration and several US acquisitions were performed. In a first sweep, a minimum force for US screening (5 N) was applied statically. For a second sweep, the force estimation as described in Sec. II-D was used, greatly improving the image quality as illustrated in Fig. 2. As expected [16], the confidence is dependent on the exerted force on the tissue, as visualized in Fig. 3b. In total, the estimated force $\mathbf{F_d}$ was 14.8 ± 6.4 N for all volunteers. In a final sweep (only one volunteer), we tested the capabilities of the robot controller to compensate for motion in real-time to maintain a constant force. Therefore, we asked the volunteer to perform one deep chest inhalation and then breath abdominally throughout the acquisition. Results show that the force controller maintained the desired force with an average error of 0.17 ± 0.24 N, and that a steady acquisition of the (almost incompressible) aorta is possible while breathing.

[1] https://github.com/SalvoVirga/iiwa_stack
[2] http://www.ros.org/

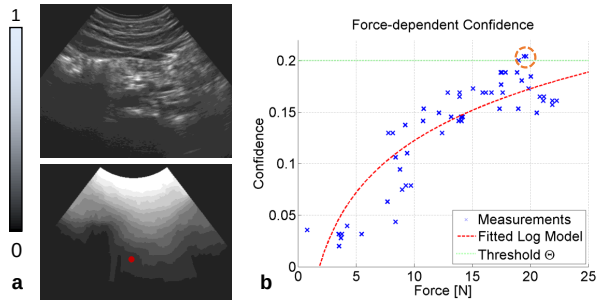

Fig. 3. **a)** Exemplary B-mode frame of the aorta, corresponding confidence map, and expected center of the aorta (*red*). **b)** Confidence values at the depth of the aorta during initial force estimation for one representative subject, showing a degressive dependency on the exerted force. The final force of 20 N was reached after the confidence exceeded $\Theta = 0.2$ (*circled*).

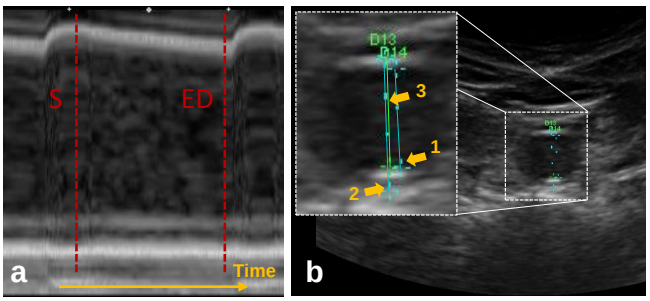

Fig. 5. Result of manual measurement as in clinical routine. **a)** M-mode frame showing cross-section of the aorta over time, allowing for the selection of B-mode frames corresponding to systole (*S*) and end-diastole (*ED*). **b)** B-mode frame with zoomed window of the aorta, showing how inner (*1*), outer (*2*), and leading-edge diameters (*3*) were determined.

C. Optimization of Out-of-plane Rotation

In a next set of experiments, we evaluated the impact of the proposed out-of-plane rotation estimation. A first US sweep was performed with static rotation, i.e. $\alpha = 0$. A representative case is depicted in Fig. 4. In particular in the beginning of the sweep, shadowing artifacts made the aorta not detectable. In contrast, the initial rotation estimation for a second sweep determined an optimal angle of $\alpha = 9.2°$, which led to a significantly increased confidence within the first 30 mm of the sweep. For the remaining trajectory, our controller gradually lowered the out-of-plane rotation and maintained high confidence. For all subjects, the optimal initial rotation was found to be $\alpha_0 = 3.2 \pm 8.0°$.

D. Aortic Diameter Measurements

In all five volunteers, the aortic diameter was measured by a medical expert in the compounded US volumes in sagittal and axial slices according to the guidelines in [4]. For comparison, a medical expert blind to formerly mentioned measurements performed a standard US scan on each volunteer according to the clinical protocol as in [7] (see Fig. 5). In particular, inner diameters d_{in} (without walls), outer diameters d_{out} (with walls) and leading-edge diameters d_{le} (with closer wall only) were measured. Table I reports the results obtained in both scenarios. On average, the error between manual US scan measurement and the ones performed in the robotically acquired volumes was 0.5±0.3 mm.

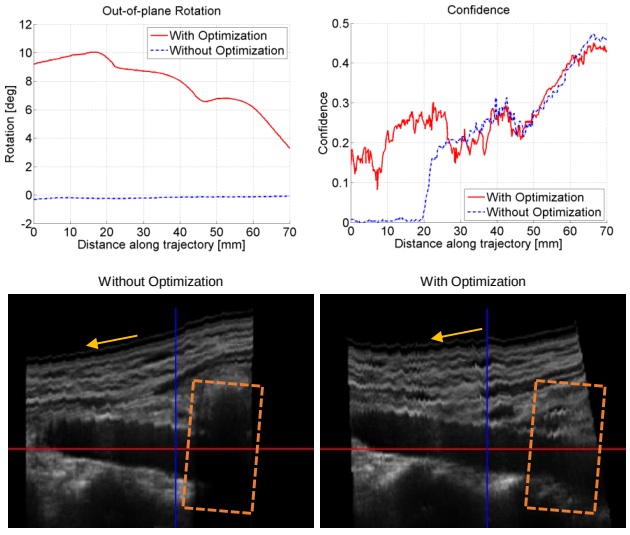

Fig. 4. Comparison between static out-of-plane rotation and optimization based on confidence for one representative subject. The proposed method avoids the shadowing in the beginning of the trajectory (*orange box*). Throughout the acquisition, optimization of the rotation (*top left*) maintains high confidence (*top right*). Yellow arrows indicate the scan direction.

IV. DISCUSSION

With regards to the aortic diameter measurement, our results indicate that the proposed framework allows for the same quantitative measurements as obtained in current clinical practice (cf. Tab. I). The results also validate the adaptive choice of the optimal contact force for the procedure, as the values estimated by our method resulted in a superior image quality. A low force would have led to an overall less visible aorta, while a too high force could have compressed it, thus affecting the diameter measurements. Additionally, the high standard deviation of our automatic force estimation shows the importance of a patient-specific pressure estimation. It should be noted that in this work, all volunteers were within a close range of age and physique, such that much higher variations of various tissues layers can potentially impact the overall ultrasound image quality and contact force for more diverse patient populations. It is further interesting that a good imaging of the aorta was also possible under normal patient breathing (cf. Fig. 2). This might open up the way for optimizations of the current acquisition protocol, in the prospect of a system exploiting normal breathing. With respect to the out-of-plane rotation of the transducer,

TABLE I
AVERAGE DIAMETER MEASUREMENT RESULTS [MM] (5 SUBJECTS)

	Robotic Scan		Manual Scan		Error	
	S	ED	S	ED	S	ED
d_{in}	13.50	11.68	13.38	11.58	0.32±0.13	0.54±0.22
d_{out}	16.68	15.00	16.68	14.84	0.48±0.28	0.56±0.34
d_{le}	15.08	13.34	15.00	13.08	0.52±0.38	0.46±0.15

obtained results demonstrated that the choice of an optimal angle at the beginning, coupled with an ongoing optimization throughout the sweep, leads to an overall improved image quality (cf. Fig. 4). This is in line with clinical practice, where the transducer is regularly tilted to avoid bowel gas and to follow a potential curvature of the aorta [7]. It needs to be noted, however, that reaching and maintaining the globally optimal orientation is not guaranteed by the control scheme. A more in-depth analysis of control stability and confidence convergence is suggested for future studies.

Finally, the presented system allows for a further extension to other applications, such as more complex diagnostic procedures in the vascular domain. Beyond that, the system could facilitate a broader implementation of robotic systems for repetitive and already standardized medical practices.

V. CONCLUSION

In this work, we introduced a fully autonomous robotic system aimed at ultrasound screening for abdominal aortic aneurysms. We have demonstrated a generalized approach to cope with the large variety of anatomies involved in a screening program. Our results show improved quality of 3D US acquisitions, and the clinical validation shows comparable diameter measurements to the ones obtained following current standard of care. This work demonstrates the potential impact of robotic systems on the medical domain, especially in contexts demanding flexibility and adaptation to individual patients. We believe that the generality of the system, based on the foundations of prior work, enables its extension to additional clinical applications and further helps to promote the use of robotic systems in standard medical care.

ACKNOWLEDGMENT

This work was partially supported by KUKA Roboter GmbH, Augsburg, Germany, and Bayerische Forschungsstiftung award number AZ-1072-13 (RoBildOR). We thank ImFusion GmbH, Munich, Germany, for providing their image processing framework and their continuous support.

REFERENCES

[1] T. H. Wong, K. H. Tay, M. G. Sebastian, and S. G. Tan, "Duplex ultrasonography arteriography as first-line investigation for peripheral vascular disease." *Singap Med J*, vol. 54, no. 5, pp. 271–274, 2013.

[2] A. Nchimi, J. Biquet, D. Brisbois, P. Reginster, K. Bouali, C. Saive, and P. Magotteaux, "Duplex ultrasound as first-line screening test for patients suspected of renal artery stenosis: prospective evaluation in high-risk group," *Eur Radiol*, vol. 13, no. 6, pp. 1413–1419, 2003.

[3] D. C. Brewstera, J. L. Cronenwett, J. W. Hallett, K. W. Johnston, W. C. Krupski, and J. S. Matsumura, "Guidelines for the treatment of abdominal aortic aneurysms: report of a subcommittee of the joint council of the american association for vascular surgery and society for vascular surgery," *Vascular Surg*, vol. 37, no. 5, pp. 1106–1117, 2003.

[4] W. Schäberle, L. Leyerer, W. Schierling, and K. Pfister, "Ultrasound diagnostics of the abdominal aorta," *Gefässchirurgie*, vol. 20, no. 1, pp. 22–27, 2015.

[5] L. Beales, S. Wolstenhulme, J. Evans, R. West, and D. Scott, "Reproducibility of ultrasound measurement of the abdominal aorta," *Brit J Surg*, vol. 98, no. 11, pp. 1517–1525, 2011.

[6] P. De Rango, "Aneurysm diameter measurement: A challenging and frustrating task," *Eur J Vasc Endovasc*, vol. 43, no. 1, p. 34, 2012.

[7] K. Pfister, W. Schierling, E. M. Jung, H. Apfelbeck, C. Hennersperger, and P. M. Kasprzak, "Standardized 2D ultrasound versus 3D/4D ultrasound and image fusion for measurement of aortic aneurysmdiameter in follow-up after EVAR," *Clin Hemorheol Micro*, pp. 1–13, 2015.

[8] T. Schmidt, N. Mühlberger, I. Chemelli-Steingruber, A. Strasak, B. Kofler, A. Chemelli, and U. Siebert, "Benefit, risks and cost-effectiveness of screening for abdominal aortic aneurysm." *Fortschr Geb Rontgenstrahlen Nuklearmed Erganzungsbd*, vol. 182, no. 7, pp. 573–580, 2010.

[9] K. Evans, S. Roll, and J. Baker, "Work-related musculoskeletal disorders (WRMSD) among registered diagnostic medical sonographers and vascular technologists: a representative sample," *J Diagn Med Sonogr*, 2009.

[10] A. Fenster, D. B. Downey, and H. N. Cardinal, "Three-dimensional ultrasound imaging," *Phys Med Biol*, vol. 46, no. 5, p. R67, 2001.

[11] A. Gee, R. Prager, G. Treece, and L. Berman, "Engineering a freehand 3D ultrasound system," *Pattern Recognit Lett*, vol. 24, no. 4, pp. 757–777, 2003.

[12] K. Bredahl, N. Eldrup, C. Meyer, J. Eiberg, and H. Sillesen, "Reproducibility of ECG-gated ultrasound diameter assessment of small abdominal aortic aneurysms," *Eur J Vasc Endovasc Surg*, vol. 45, no. 3, pp. 235–240, 2013.

[13] C. Hennersperger, A. Karamalis, and N. Navab, "Vascular 3D+T freehand ultrasound using correlation of doppler and pulse-oximetry data," in *Information Processing in Computer-Assisted Interventions*, 2014, pp. 68–77.

[14] E. M. Boctor, M. A. Choti, E. C. Burdette, and R. J. Webster Iii, "Three-dimensional ultrasound-guided robotic needle placement: an experimental evaluation," *Int J Med Robot*, vol. 4, no. 2, pp. 180–191, 2008.

[15] C. Nadeau and A. Krupa, "Intensity-based ultrasound visual servoing: Modeling and validation with 2-d and 3-d probes," *Robotics, IEEE Transactions on*, vol. 29, no. 4, pp. 1003–1015, 2013.

[16] P. Chatelain, A. Krupa, and N. Navab, "Confidence-driven control of an ultrasound probe: Target-specific acoustic window optimization," in *Robotics and Automation, 2016 IEEE Int. Conference on*, 2016.

[17] O. Zettinig, B. Fuerst, R. Kojcev, M. Esposito, M. Salehi, W. Wein, J. Rackerseder, B. Frisch, and N. Navab, "Toward real-time 3D ultrasound registration-based visual servoing for interventional navigation," in *Robotics and Automation, 2016 IEEE Int. Conference on*, 2016.

[18] B. Mustafa, A. Safwan, T. Ishii, Y. Matsunaga, R. Nakadate, H. Ishii, K. Ogawa, A. Saito, M. Sugawara, K. Niki *et al.*, "Development of robotic system for autonomous liver screening using ultrasound scanning device," in *Robotics and Biomimetics, 2013 IEEE International Conference on*, 2013, pp. 804–809.

[19] C. Hennersperger, B. Fuerst, S. Virga, O. Zettinig, B. Frisch, T. Neff, and N. Navab, "Towards MRI-based autonomous robotic US acquisitions: A first feasibility study," *arXiv preprint arXiv:1607.08371 [cs.RO]*, 2016.

[20] A. Karamalis, W. Wein, T. Klein, and N. Navab, "Ultrasound confidence maps using random walks," *Med Image Anal*, vol. 16, no. 6, pp. 1101–1112, 2012.

[21] M. Reyes, M. A. G. Ballester, Z. Li, N. Kozic, R. M. Summers, and M. G. Linguraru, "Anatomical variability of organs via principal factor analysis from the construction of an abdominal probabilistic atlas," in *2009 IEEE International Symposium on Biomedical Imaging: From Nano to Macro*, 2009, pp. 682–685.

[22] A. Myronenko, X. Song, and M. A. Carreira-Perpinán, "Non-rigid point set registration: Coherent point drift," in *Adv Neural Inf Process Syst*, 2006, pp. 1009–1016.

[23] C. Schulte zu Berge, D. Declara, C. Hennersperger, M. Baust, and N. Navab, "Real-time uncertainty visualization for B-mode ultrasound," in *Scientific Visualization, Proceedings on*, 2015.

[24] C. Hennersperger, D. Mateus, M. Baust, and N. Navab, "A quadratic energy minimization framework for signal loss estimation from arbitrarily sampled ultrasound data," in *Medical Image Computing and Computer-Assisted Intervention*, 2014, pp. 373–380.

[25] F. A. Fröhlich, G. Passig, A. Vazquez, and G. Hirzinger, "Robot assisted internal mammary artery detection for coronary revascularisation surgery," in *Intelligent Robots and Systems, IEEE/RSJ International Conference on*, 2010, pp. 1849–1855.

[26] M. W. Spong, "Modeling and control of elastic joint robots," *J Dyn Syst Meas Control*, vol. 109, no. 4, pp. 310–318, 1987.